Chapter 2

Experimental Methods

Experiments were performed on six floors: three laboratory specimens, one full-scale mockup, and two buildings under construction. The objective was to obtain estimates of modal properties that affect floor acceleration response and to determine the response to walking excitation. A series of footstep force measurements was performed toward the goal of defining reasonable forcing functions to be applied during finite element modeling. This chapter contains brief descriptions of the specimens (detailed descriptions are in Chapter 4) and descriptions of the experimental methods, measurement details, and post-processing methods. Results of the experimental program are presented and compared with analytical predictions in Chapter 4.

2.1 Specimen Descriptions

2.1.1 Long Span Composite Slab Laboratory Specimen

A long span composite slab specimen was built and tested at the Virginia Tech Structures and Materials Research Laboratory in 2006. It consisted of an 8-3/4 in. thick shored composite slab supported only by perimeter beams and girders. The 30 ft by 30 ft specimen is shown in Figure 2.1.

Figure 2.1: Long Span Composite Slab Laboratory Specimen

2.1.2 Square-End Joist Footbridge Laboratory Specimen

A 30 ft by 7 ft steel joist footbridge laboratory specimen was built and tested at the Virginia Tech Structures and Materials Research Laboratory in 2005 and 2006. It consisted of a 6-1/2 in. thick composite slab supported on bottom chord bearing open-

web steel joists. The bridge was built in three stages, but only the first is included in this research. Stage 1 was a nominally simply-supported footbridge as shown in Figure 2.2.

Figure 2.2: Shear Connected Joist Footbridge Laboratory Specimen

2.1.3 Shear-Connected Joist Footbridge Laboratory Specimen

A 90 ft by 7 ft steel joist footbridge laboratory specimen was built and tested at the Virginia Tech Structures and Materials Research Laboratory in 2006. It consisted of a 6-1/2 in. thick composite slab supported on open-web steel joists with shear connections rather than typical joist seats. Figure 2.3 shows photographs of the specimen and a representative joist shear connection.

2.1.4 Long Span Composite Slab Mockup

A 61 ft by 74 ft full-scale floor mockup was built and tested in Las Vegas in January 2008. It used the same shored 8-3/4 in. composite slab system as described above. The slab was supported by perimeter beams and interior girders to simulate a four bay portion of a hotel wing with 30 ft by 30 ft areas free of columns and beams. Figure 2.4 is a picture of the mockup.

Figure 2.3: Shear-Connected Joist Footbridge Specimen

Figure 2.4: Long Span Composite Slab Mockup

2.1.5 Riverside Medical Office Building (Riverside MOB)

A large portion of the second elevated floor of a building under construction was tested in Roanoke, Virginia in 2006. The floor was constructed using conventional composite slabs (5-1/2 in. total on 2 in. deck) and wide-flange beams and girders. It was mostly clear of construction material, piping, ceiling, etc. at the time of testing. The tested bays were 30 ft by 30 ft. Figure 2.5 shows photographs of the structure.

Figure 2.5: Riverside Medical Office Building

2.1.6 First Bank and Trust Building

The top floor of a building under construction was tested in Christiansburg, Virginia in 2006. The floor was constructed using a thin non-composite slab on form deck, supported by conventional open-web steel joists at a close spacing. The floor was mostly free of construction material, piping, etc. at the time of testing. Bay sizes varied, but were approximately 20 ft by 30 ft. See Figure 2.6 for pictures of the structure.

Figure 2.6: First Bank and Trust Building

2.2 Experiments to Determine Modal Properties

Experimental modal analysis (EMA) techniques were used to estimate modal properties that affect a floor response to walking (natural frequencies, mode shapes, damping), and acceleration response to sinusoidal load. In general, the same techniques were used as described by Avci (2005) and Barrett (2006). Measured force input (excitation) was supplied by an electrodynamic shaker and accelerations (responses) were measured at various locations on the slab. These measured time domain signals were used to estimate the accelerance frequency response functions (FRFs) for response and excitation at various locations on the slab.

FRFs are commonly presented as the complex ratio of displacement, velocity, or acceleration to applied force. Acceleration is the most convenient for floor vibrations because it is the quantity most often used to evaluate acceptability and because it is directly measured during experiments. Therefore, the accelerance (ratio of acceleration response to force input) is displayed throughout this dissertation. The accelerance can be displayed in in./sec.^{2}/lbf, m/sec.^{2}/N, g/lbf, g/N, %g/N, or any other choice of acceleration units per force units. In this research, %g/lbf is used because it is the most consistent with DG11 and because of its resemblance to usual engineering design units. The FRF, being a complex quantity, contains magnitude and phase information. While the phase plot also contains useful information, the magnitude is typically of primary interest (Ewins 2008) and is displayed throughout this dissertation. A sample accelerance FRF magnitude is shown in Figure 2.7. The FRF has numerous interesting properties. For example, the imaginary part of the FRF at a natural frequency is in direct proportion to

the mode shape at the measurement location, even indicating the sign. This is obviously very useful for quality control during modal tests.

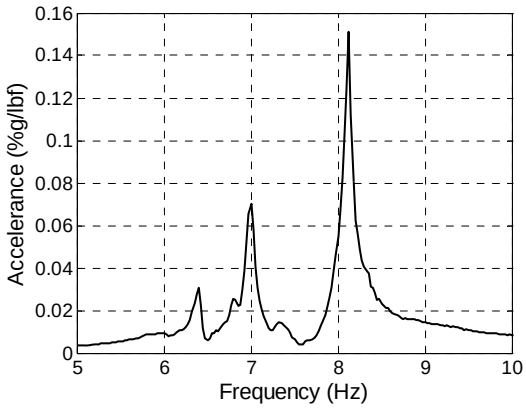

Figure 2.7: Sample Accelerance Frequency Response Function

FRFs were used in this research to determine modal properties. This section contains a detailed description of these experiments and post-processing. For an in-depth discussion of modal testing of floors, see Barrett (2006).

2.2.1 Measurement of Excitation and Response

An APS Dynamics Electro-Seis Model 400 electrodynamic shaker (Figure 2.8) was used to provide excitation for modal tests. A shaker was chosen, rather than an impulse hammer or other exciter, because it allows higher quality FRFs to be measured (Pavic and Reynolds 1999, Reynolds and Pavic 2000a, Reynolds and Pavic 2000b, Hanagan et al. 2003, Barrett 2006).

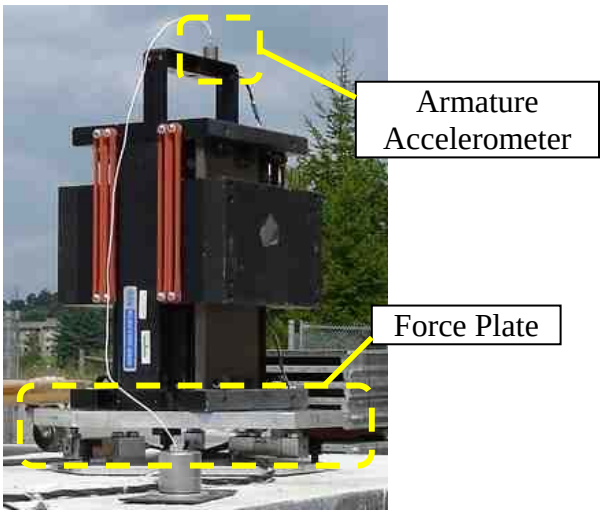

Figure 2.8: Electrodynamic Shaker

Burst chirp (sinusoid with approximately constant amplitude and continuously varying frequency) excitation was used because it provides an excellent signal-to-noise ratio (Reynolds and Pavic 2000a, Hanagan et al. 2003, Mayes and Gomez 2006) and precise control over the level of force and frequency content delivered to the structure (Ewins 2000). A chirp force waveform is shown in Figure 2.9. As is seen from viewing the autospectrum (DFT times the complex conjugate of DFT at each spectral line), the main feature of a chirp excitation is a fairly constant force input at all frequencies in the swept bandwidth (approximately 3.25 Hz to 6.75 Hz in Figure 2.9). For all tests, chirp frequency was varied from low to high, although it is also possible to vary the frequency from high to low. The start and end frequencies were selected to encompass any structural natural frequencies of interest, with at least 1 Hz below and above the lowest and highest frequency of interest, respectively. The duration of the force and overall record length were selected to allow the structural vibrations to decay to very low levels between subsequent records. Digital signal processing settings were selected to provide a fine frequency resolution, 0.0125 Hz or 0.025 Hz, using a 20 Hz bandwidth and 40 sec. or 80 sec. capture time, as time permitted.

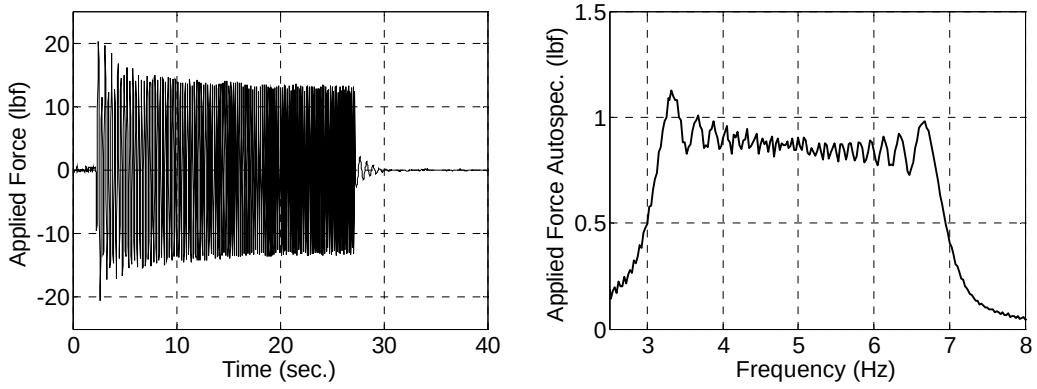

Figure 2.9: Sample Burst Chirp Forcing Function. (a) Waveform; (b) Autospectrum

The force amplitude was selected to result in peak accelerations approximately equal to those expected during subsequent walking tests—approximately 0.5%g to 2.0%g. All structures exhibit some amount of nonlinearity even at low vibration levels, so it is not possible to select a "correct" force level. However, for the tested floors, the results were not sensitive to force level selection in the range listed above. For example, consider the measured FRFs shown in Figure 2.10. The FRF magnitudes differed by

approximately 7% which is significant, but not a wide enough margin to make one or the other measurement unreasonable for use in the subsequent comparison with analytical predictions. It is the writer's experience that difficulties associated with nonlinearities during floor vibration modal tests occur when the force levels are varied over a much wider range than used throughout this research and when large force drop-offs occur due to shaker-structure interaction.

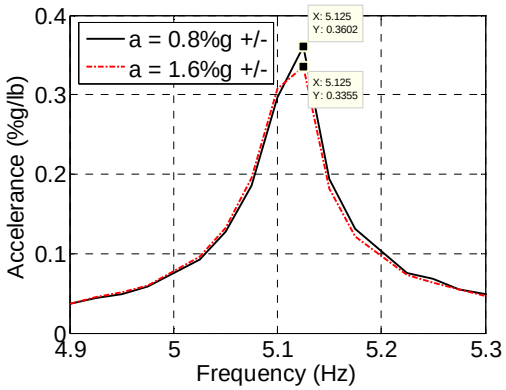

Figure 2.10: Sample FRF Illustrating Effect of Force Level

Whenever possible, the applied force was directly measured using a custom-built force plate placed under the shaker, also shown in Figure 2.8. The alternative force measurement method is to use an armature accelerometer for an indirect force measurement, assuming that the force delivered to the slab is equal to the armature mass times its acceleration. This method only works well if the structure is very massive in comparison to the armature (Davis et al. 2007). Force drop-offs inevitably occur as the chirp signal passes through structural natural frequencies but these drop-offs are not detected by viewing an armature accelerometer waveform as shown in Figure 2.11. The consequence of these drop-offs, so-called "force glitches" in the autospectrum, are also shown in Figure 2.11. The force autospectrum computed from the armature accelerometer signal completely misses the force glitch, which is unacceptable because the force autospectrum is directly used in estimation of the FRF. For grounded structures such as the ones in this research, the size of these force glitches depends on the structure-to-armature mass ratio (Davis et al. 2007), ranging from very severe for light laboratory specimens to very minor for relatively massive structures. The force glitch size can also

be reduced by placing the shaker at a location on the structure with a lower accelerance FRF magnitude as shown in Figure 2.12.

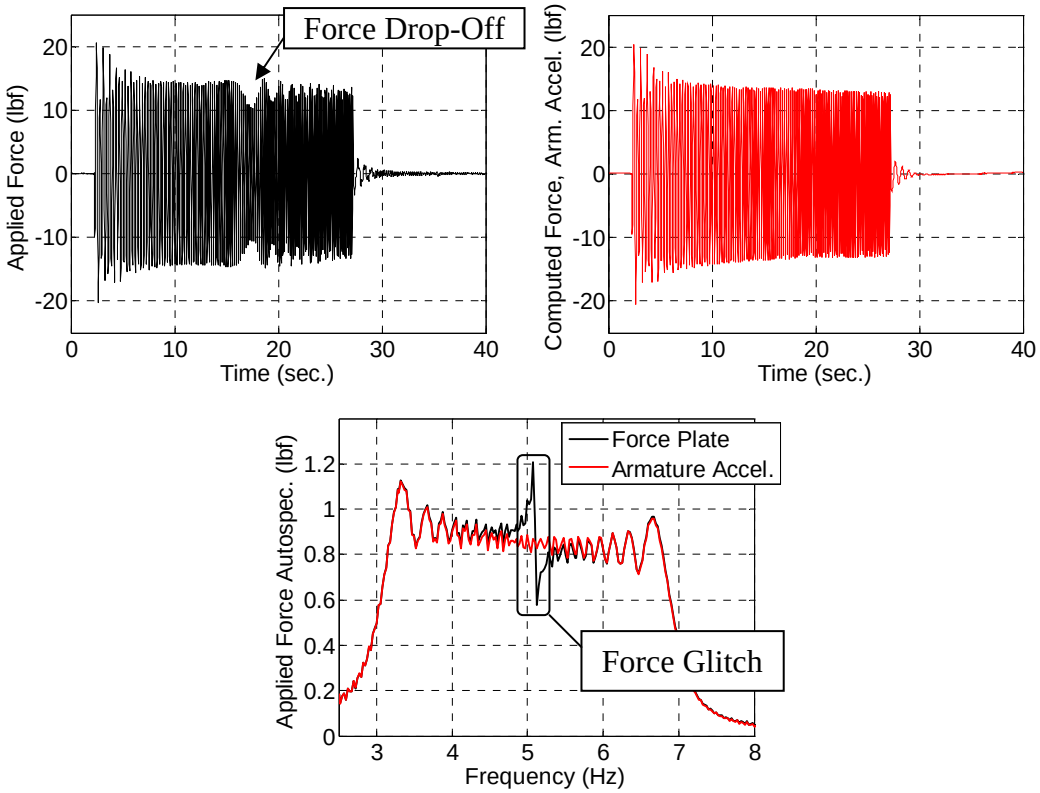

Figure 2.11: Chirp Excitation Showing Force Drop-Off. (a) Measured Using Force Plate; (b) Measured Using Armature Accelerometer; (c) Force Autospectrum

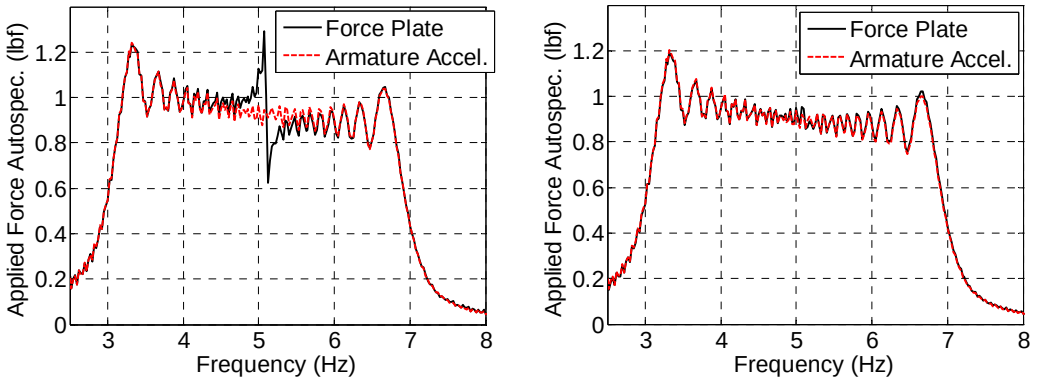

Figure 2.12: Force Autospectra—Same Structure and Armature Mass. (a) Shaker at Mid-Bay; (b) Shaker at Edge.

Minimization of force glitches is also important when using the force plate to measure the applied forces, although the consequences are not as severe as when using the armature accelerometer. The issue is illustrated using Figure 2.13, which shows the

acceleration autospectrum, force autospectrum, and resulting accelerance magnitude. The accelerance magnitude is equal to the spectral line-by-line quotient of the acceleration autospectrum and the force autospectrum. The acceleration autospectrum is necessarily very narrow and steep near a structural natural frequency for lightly damped structures. With the presence of a force glitch, the force autospectrum is also very steep at and just below the structural natural frequency. The resulting accelerance magnitude is the quotient of these two very rapidly changing functions, resulting in poor test-to-test repeatability regardless of the level of care, number of averages, force level, or force measurement method employed during testing. Therefore, the best quality measurements are acquired if force glitches are minimized either by reducing the armature mass or moving the shaker to a point on the structure with lower accelerance magnitude.

For the floors included in this study, the highest quality modal results were obtained for floors with high structure-to-armature mass ratios. The two light joist footbridge specimens had fairly low structure-to-armature mass ratios and the issues described in the preceding paragraphs were not well understood at the time of testing. The modal results for the footbridge tests appear to be of high enough quality for use in this research, however.

Acceleration responses at locations of interest were measured using PCB Model 393C accelerometers produced by PCB Piezotronics. One accelerometer was placed as close as possible to the shaker for a driving point measurement. Other accelerometers were "roved" across a sufficient number of degrees-of-freedom (DOF) to allow later definition of the mode shapes. The grid of DOF was finer for the laboratory specimens than for the building floors, at supports and quarter points versus at the middles of bays only. As reported by Barrett (2006), a finer grid is only useful to allow viewing of higher frequency mode shapes with double curvature. These higher frequency modes are of little interest for floor vibrations in general and are well outside the frequency bandwidth of interest for all of the floors in this study. Therefore, coarser grids were chosen for the Riverside MOB and First Bank and Trust simply due to time constraints. (The entire testing program, including setup and packing, had to be completed within approximately 8-10 hours at each site.)

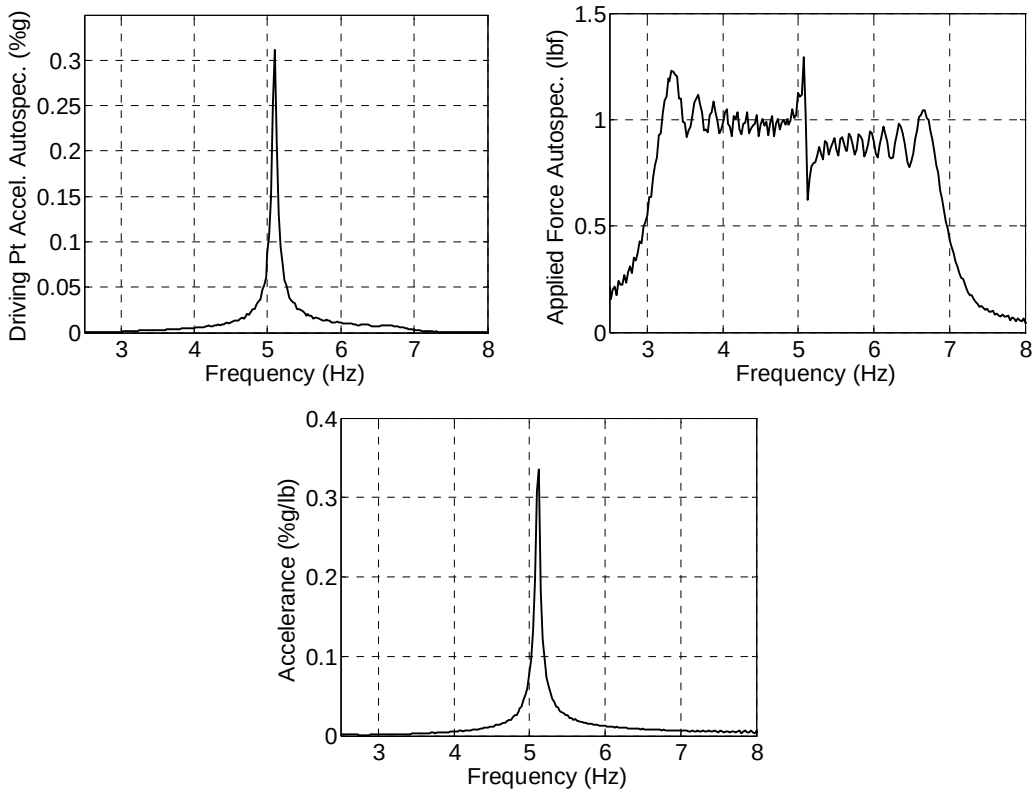

Figure 2.13: Driving Point Acceleration, Force, and Resulting Accelerance FRF Magnitude

The accelerometers were placed on rubber pads as shown in Figure 2.14. Barrett (2006) verified during laboratory tests that it is not necessary to mechanically fasten this type of accelerometer to a horizontal floor slab during low-acceleration tests such as those performed in this research. The anticipated vertical accelerations (5%g, maximum) are insufficient to cause uplift and the wide, flat bases result in an automatically correct vertical orientation. However, care was taken to ensure that the accelerometers were not placed on localized bumps, screed marks, or debris, to avoid rattling.

Force plate and accelerometer signals were recorded and analyzed using either one or two Model 20-42 Siglab digital signal processing units, shown to the left of Figure 2.15. These units also sent chirp signals to the shaker amplifier.

Figure 2.14: Accelerometers

Figure 2.15: Siglab Digital Signal Processing Units

2.2.2 FRF Estimation

EMA techniques were used to estimate the FRFs for each structure. The overall goal of EMA is to use the time domain signals (excitation and response) to produce an estimate of the FRF that can then be used to determine natural frequencies, mode shapes, damping, and acceleration response to sinusoidal load as a function of frequency. FRFs or modal properties are not measured, but are *inferred* or *estimated* from the measured time domain signals. However, in the literature and in this dissertation, the terms "measured" and "estimated" are used interchangeably.

The general input/output model used to estimate the FRF is shown in Figure 2.16 where the total force input, *F(f)* is composed of the correlated (measured) input and the

uncorrelated (unmeasured) input, *m(f)*. The total acceleration output, *Y(f)* is composed of the correlated output and the uncorrelated output, *n(f)* (Wicks 2006). Various assumptions can be made on the uncorrelated input and output. The most common assumption is that the uncorrelated content is all contained in the output and that there is no uncorrelated input. This results in the "H_1 FRF Estimator" which was used in this research. (The H_2 FRF Estimator is derived assuming all uncorrelated content is in the input and none on the output.)

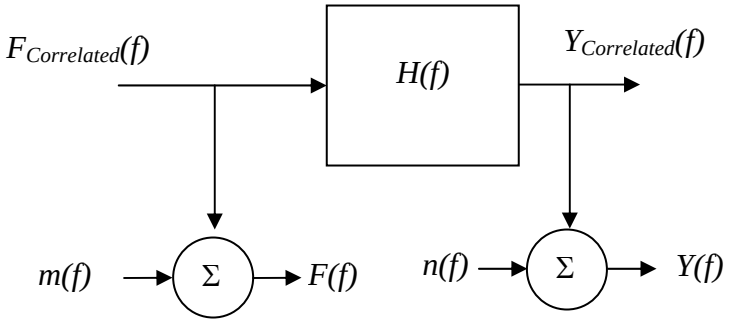

Figure 2.16: General Input/Output Model

Assuming *m(f)* = 0 and minimizing *n(f)* over an ensemble of several records presumably yields the best estimate of the FRF during modal tests with no uncorrelated input force. After considerable manipulation, the resulting equation for the estimated FRF at frequency *f* is

$$H_1(f) = \frac{G_{FY}(f)}{G_{FF}(f)} \qquad \text{(Eq. 2.1)}$$

where

G_{FY} = Cross-spectrum of the output with the input.
G_{FF} = Autospectrum of the force input.

The detailed mathematics are found in Wicks (2006). Also, see Barrett (2006) for more information on the H_1 FRF estimator. The key points are

- The cross-spectrum is a complex quantity at each spectral line whereas the autospectrum is a real quantity. The resulting FRF estimate is therefore a complex quantity at each spectral line, containing magnitude and phase information.

- The H_1 estimator assumes that uncorrelated content exists in the output acceleration. The accuracy of the estimate depends on the number of records contained in the ensemble. A larger number of records allows better minimization of the effects of uncorrelated output. For the floors included in this research, ensembles of three records (also referred to as "three averages") was found to provide a good compromise of sufficient accuracy for the time spent.
- The H_1 estimator assumes no uncorrelated input. In other words, if the input force has significant uncorrelated content, the algorithm has no way to minimize its effects on the FRF estimate, regardless of the number of records in the ensemble. This emphasizes the importance of clean and accurate force measurements and the need to use a force transducer under the shaker (rather than an armature accelerometer) whenever possible.

The coherence function provides an indication of the amount of uncorrelated output so it was used during the measurements as a rough indicator of the quality of the FRF estimate. Values approaching unity indicate that no uncorrelated output exists in the FRF estimate. A sample FRF and corresponding coherence function are shown in Figure 2.17. Note the slight decrease in coherence at the anti-resonances between natural modes for this driving point FRF. As a cautionary note, it is possible to compute very high coherence at each spectral line, but still have poor quality estimates if significant uncorrelated input force exists, further emphasizing the importance of accurate force measurement.

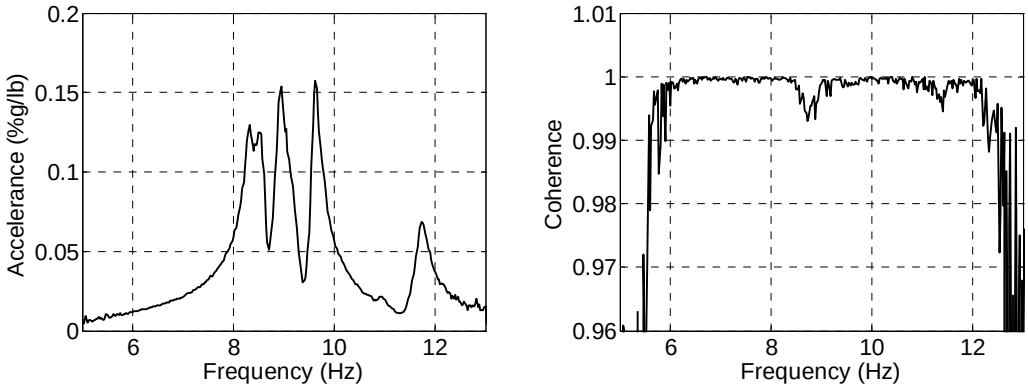

Figure 2.17: Sample FRF Magnitude and Coherence Function. (a) FRF; (b) Coherence.

2.2.3 Modal Property Extraction Using FRF Curve Fitting

FRF curve fitting was used with the main goal of determining modal damping ratios, and secondarily, to determine mode shapes. Natural frequencies and steady-state acceleration response to sinusoidal load were directly determined by observing the estimated FRF magnitudes. However, estimates of FRFs do not directly provide indications of modal damping ratios. Damping ratios also proved difficult or impossible to approximate for most of the tested floors using simpler means such as log decrement or half-power bandwidth due to the presence of multiple modes. Therefore, FRF curve fitting using ME'ScopeVES Version 3.0 (Vibrant Technology 2003) was performed to obtain these key quantities. Also, as previously mentioned, mode shapes can be approximated by observing the imaginary part of the FRF at natural frequencies, but this is cumbersome, does not provide illustrative plots, and does not indicate whether a mode shape is real, quasi-real, or complex. Therefore mode shapes were also approximated using FRF curve fitting.

The basic concept of FRF curve fitting is to attempt to match a parametric mathematical model of the system (composed of several modes with specific frequencies, damping ratios, and mode shape components) with a series of estimated FRFs. A sample curve-fit FRF is shown in Figure 2.18. If the re-synthesized FRFs from the mathematical model closely resemble the estimated FRFs, then the set of assumed natural frequencies, damping ratios, and mode shape components approximate those of the actual system.

Several options are available within ME'ScopeVES for use during curve fitting operations. FRF curve fitting can be done on a global or local basis, using all estimated

FRFs in a measurement set (modal sweep) simultaneously or on a FRF-by-FRF basis, respectively. Global curve fitting was used throughout this research. Modes can be indicated using one of three methods: Modal Peaks Function, Complex Mode Indicator Function, and Multivariate Mode Indicator Function. Because curve fitting was performed on sets of FRFs with the same reference, the Modal Peaks Function was used. ME'ScopeVES provides several methods for determining the parameters of the mathematical model, including Global Polynomial (usually used in this research), Complex Exponential, Co-Quad, and Peak. Results from various methods were compared, when appropriate (Co-Quad and Peak are SDOF methods so were not used, for example). The General Polynomial Method usually produced synthesized FRFs that were reasonable matches to the estimated FRFs. However, manual manipulation of the modal frequencies and damping ratios consistently produced much better matches.

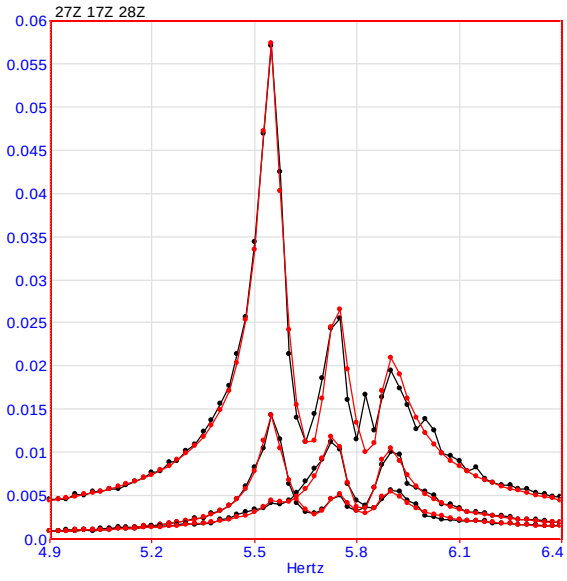

Figure 2.18: Sample Curve-Fit FRF (Black = Estimated, Red = Curve-Fit)

Mode shapes were also determined using the curve fitting process, indicating both the shape and complexity. Complex modes occur when damping is non-proportional (damping is concentrated at the joints for example, so is distributed much differently than are mass and stiffness) *and* when modes are closely spaced (Ewins 2000). A sample mode shape and corresponding Argand "starburst" plot are shown in Figure 2.19. The starburst plot indicates no complexity if all of the vectors are parallel to each other. If the vectors fall within approximately 10 deg. of each other, then the mode is quasi-real

(Ewins 2008), which was seen during most of the presented results. In most cases, the DOF which were significantly out of phase with the others were subject to very little excitation, so the modal results should be considered suspect for those DOFs.

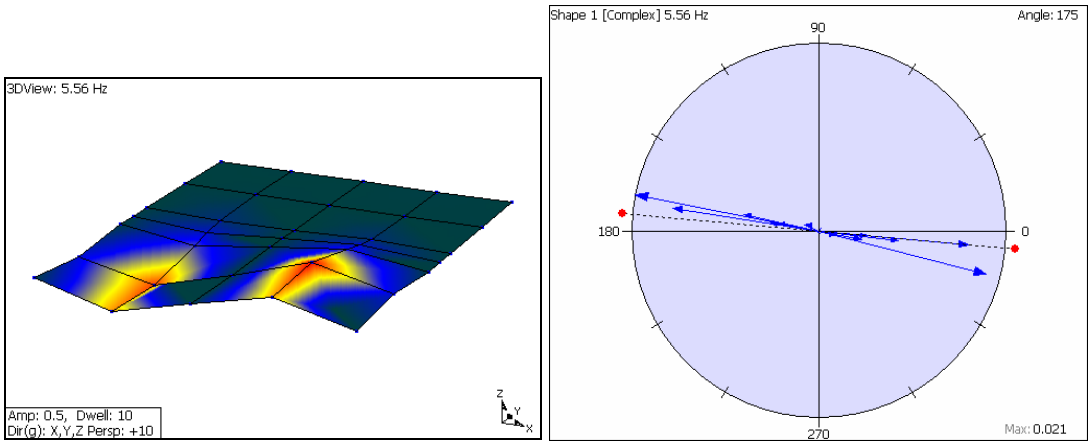

Figure 2.19: Sample Mode Shape and Starburst Plot

2.3 Experiments to Determine Response to Walking

Experiments were also performed to determine the acceleration response to walking excitation for each floor. The general approach was to first use modal tests to estimate the FRF in the bay under consideration and use it to determine which modes will provide the highest accelerations if excited. A walker then attempted to walk at resonant frequencies to determine the maximum acceleration response that can be reasonably expected for the bay, as shown in Figure 2.20.

In most cases, one mode (not necessarily the fundamental mode) had a significantly larger FRF peak magnitude, indicating that it will provide much higher accelerations than the other modes. Such a mode is referred to as the bay's "dominant mode." For example, in Figure 2.7, the dominant mode is approximately 8.1 Hz. In all cases, the dominant modal frequency was far outside the range of reasonable walking frequencies (approximately 1.6 Hz to 2.2 Hz). However, it is also possible to cause resonance using a harmonic of the walking force. Therefore, the walker carried a metronome and attempted to walk at an integer division of the dominant frequency. Accelerations were recorded at mid-bay of the tested bay and in some adjacent bays.

Multiple walking tests were performed at subharmonics of the dominant frequency and other natural frequencies which were indicated by the FRF magnitude as being responsive. Single trips across the bay under consideration were performed in

almost all cases because these are directly comparable to waveforms predicted using response history analysis. Walking paths for the laboratory specimens are obvious; those for the building floors are shown in Figure 2.21.

Figure 2.20: Walking Tests

During some of the earlier tests, walking commenced back and forth during the entire record. Except for the first trip, it is difficult to observe the resonant build-up as the walker proceeded across the bay. It is also obvious that some of the response during subsequent trips is due to decay of vibrations caused during the previous trip(s).

Four walkers, all males between 25 and 40 years old and in good health, walked on the six floors, providing a reasonable variation in loading. For all floors except the Riverside MOB and Long Span Composite Slab Mockup, the walkers wore typical athletic shoes. The Riverside MOB walker wore standard military boots and the Long Span Composite Slab Mockup walker wore hard-soled dress shoes. The choice of shoes is not of critical concern because softer shoes mainly affect higher frequencies (Kerr 1998). Galbraith and Barton (1970) also concluded that the choice of footwear and walking surface did not significantly affect the footstep force waveforms during their tests. Stride length was observed to be approximately 28 in. to 30 in. which agrees with the research by Pachi and Ji (2005).

2.3.1 Walking Acceleration Waveform Postprocessing

It is well known that human perception to floor vibration depends on the frequency of the vibration, with vibrations in the 4-8 Hz range being the most perceptible. Significant higher frequency vibrations existed in some of the waveforms due to the digital signal processing frequency bandwidth settings that were chosen, including

frequencies up to 200 Hz during some tests. Therefore, acceleration waveforms were filtered to eliminate frequency content outside the 1 Hz to 15 Hz bandwidth, the approximate frequency range of interest for human perception of walking vibration.

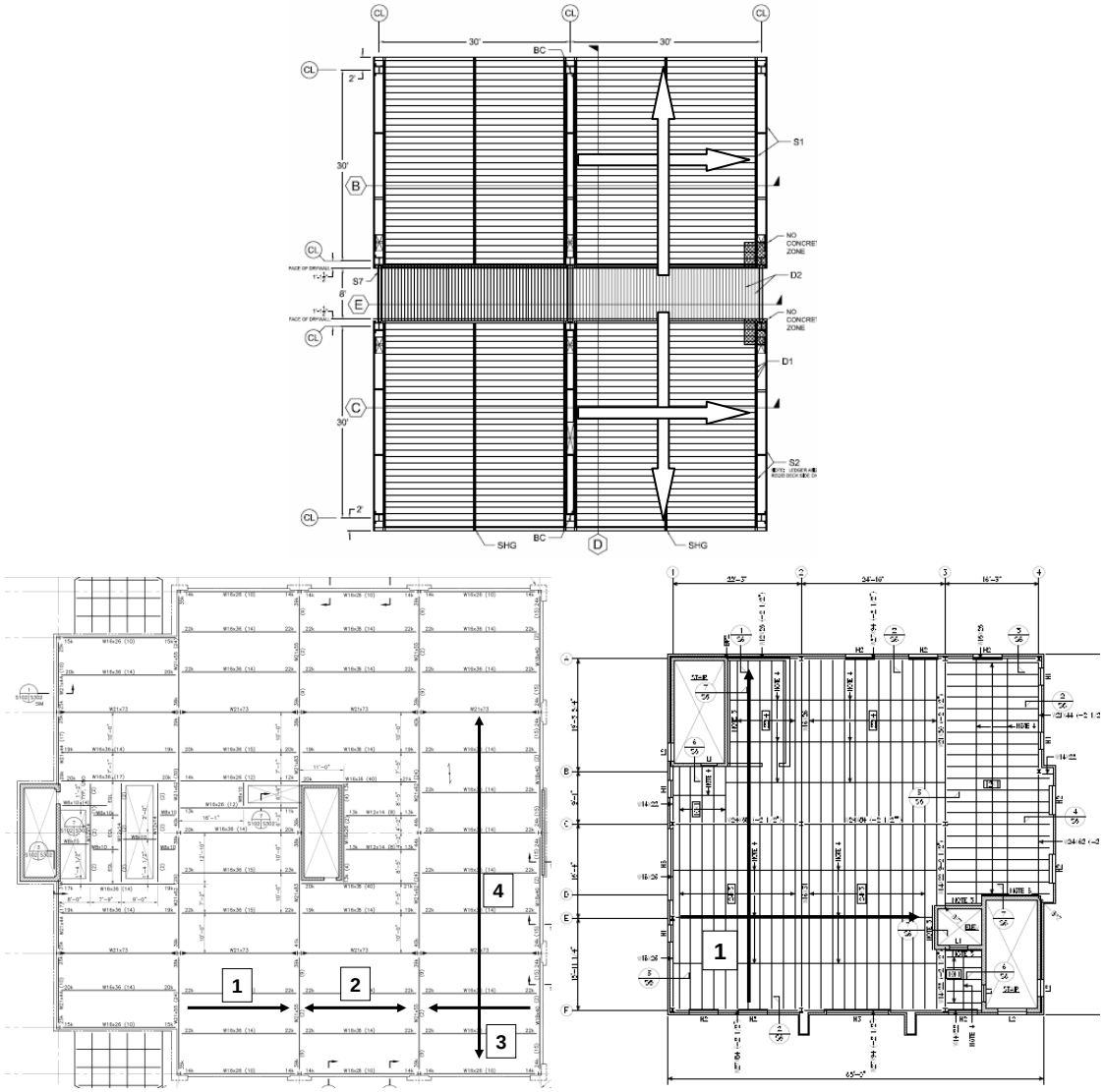

Figure 2.21: Walking Paths. (a) Long Span Composite Slab Mockup; (b) Riverside MOB; (c) First Bank & Trust.

For example, consider the measurement shown in Figure 2.22. The maximum bandwidth considered during this test was 200 Hz (chosen to allow a convenient time block length during testing), allowing sinusoids at approximately 125-150 Hz to "ride" the lower frequency signal as shown in Figure 2.22(b). Figure 2.22(d) shows the frequency content of this walking test, indicating some content in the 115-140 Hz range.

Excluding content outside the 1-15 Hz bandwidth results in a peak acceleration of 1.36%g (note that the majority of the response is due to several spectral lines around 5 Hz), which is an appropriate value for evaluating vibrations for human perception. Including all content to 200 Hz results in an apparent peak acceleration of 1.59%g, which is 17% higher than the more appropriate value.

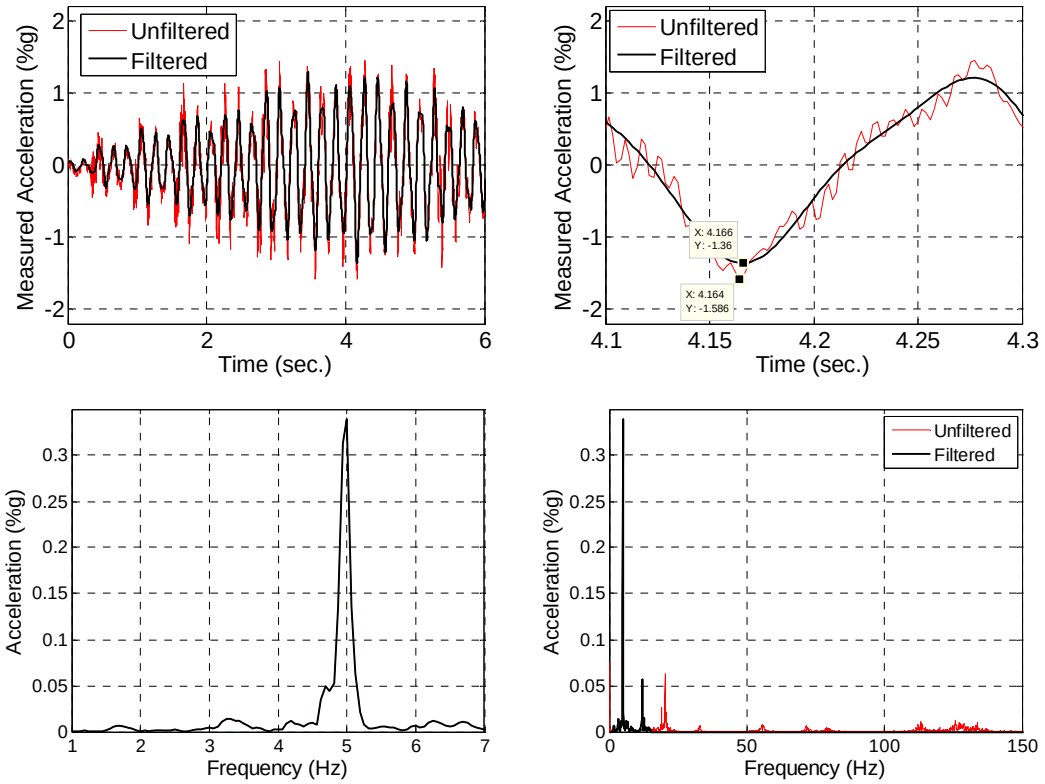

Figure 2.22: Sample Walking Acceleration Showing High Frequency Content. (a) Filtered and Unfiltered Waveform; (b) Filtered and Unfiltered Waveform Near Apparent Peak Acceleration; (c) Frequency Spectrum Showing Frequencies of Interest; (d) Frequency Spectrum Showing High Frequency Content.

It is the writer's experience that it is common for frequency content very far outside the 1-15 Hz bandwidth to have significant contributions which should be excluded. Seldom do frequencies between 15 Hz and 20 Hz have major contributions, so simply using a 20 Hz bandwidth in the DSP settings effectively eliminates most or all of the troublesome frequency content. Many of the tests performed during this research used wider bandwidths, however, so filtering during post-processing is necessary for those tests. The 1 Hz bandwidth lower limit eliminates any DC offset that may exist in the test data.

Several types of filters exist, such as Finite Impulse Response (FIR) filters and Infinite Impulse Response (IIR) filters, both of which are suitable for filtering streaming data during data acquisition or during post-processing. Because filtering of the acceleration waveform was performed during post-processing, a simpler method was used: determine the frequency content of the acceleration waveform using a Discrete Fourier Transform (via a FFT algorithm using Matlab (The MathWorks, Inc. 2006)), zero the real and imaginary parts of the sinusoids outside the 1-15 Hz bandwidth, and re-synthesize the filtered acceleration waveform using an Inverse Discrete Fourier Transform (via an IFFT algorithm using Matlab). Unlike FIR and IIR filters, a post-processing filter using the FFT / IFFT approach has no imperfection near bandwidth boundaries.

Simple sinusoids were used to successfully verify the filtering method. Also, comparisons were made with the chosen method and a FIR filter provided within Matlab, executed using the "filtfilt" command to avoid phase distortion. Figure 2.23 shows the filtered and unfiltered waveforms using the FFT/IFFT simplified filter and the FIR filter. The results are practically identical, providing more confidence in the chosen filtering method.

The final result of a walking test is a filtered waveform suitable for comparison with analytical predictions and an acceleration spectrum. A sample walking test and FRF magnitude are shown in Figure 2.24. The FRF indicates that the system has two very responsive natural modes, one at 8.3 Hz and one at 8.6 Hz. This walking test was performed at a step frequency f = 8.3 Hz / 4 = 2.08 Hz (125 bpm) in an attempt to cause resonance using the fourth harmonic of the walking force. The acceleration waveform shows a clear fourth harmonic resonant build-up. The first through third harmonics of the walking force cause very slight responses at approximately 2.1 Hz, 4.2 Hz, and 6.2 Hz and the fourth harmonic causes a very large response at 8.3 Hz (Figure 2.24(c)). The acceleration spectrum provides a good indication of the step frequency for verification during tests. Note that the 8.6 Hz mode also produced significant response, indicated by the width of the peak shown in the walking acceleration spectrum, because the footstep series applies force over a narrow bandwidth rather than precisely at the step frequency harmonic.

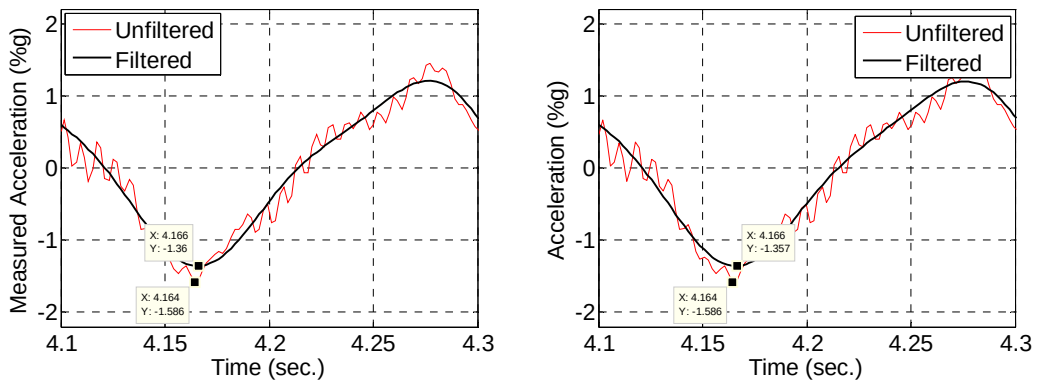

Figure 2.23: Comparison of Filtering Methods. (a) Using FFT/IFFT Filter; (b) Using FIR Filter.

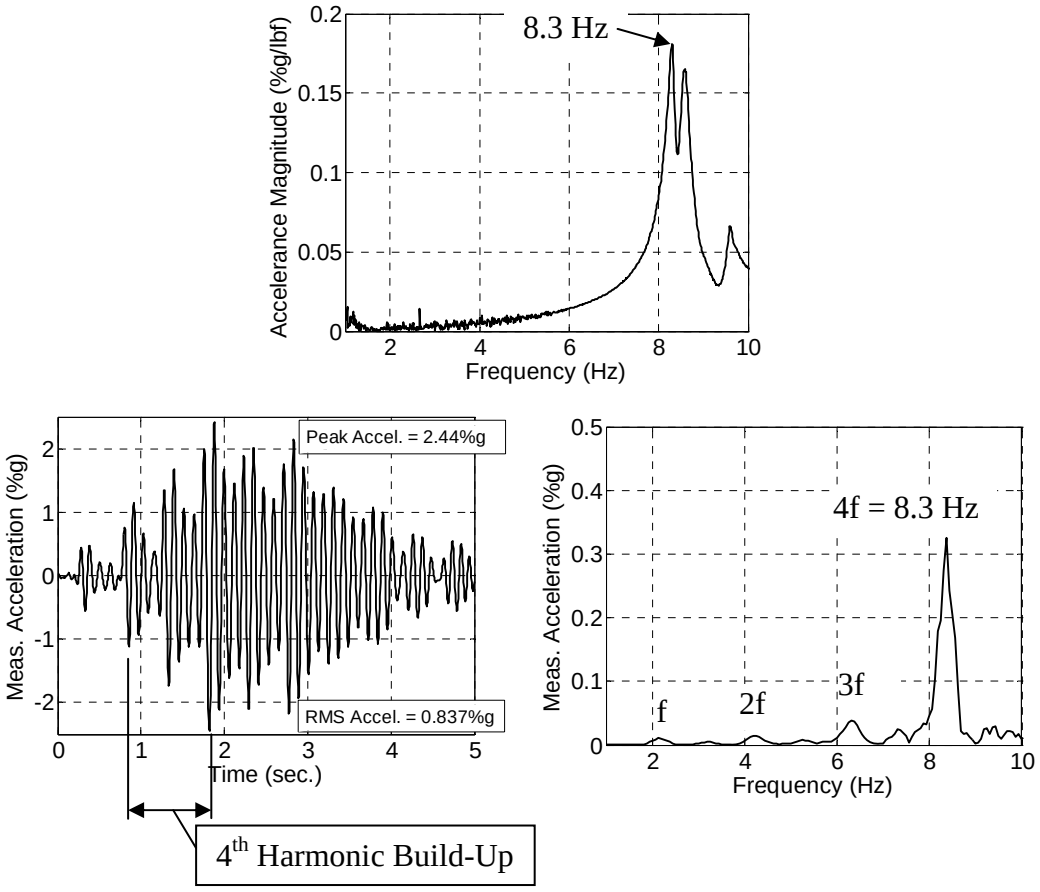

Figure 2.24: Sample Walking Test Results. (a) Accelerance Magnitude From Modal Tests; (b) Walking Acceleration Waveform; (c) Walking Acceleration Spectrum.

It is tempting to interpret the waveform shown in Figure 2.24 as indicating that the response is caused by the footstep literally striking the slab every fourth slab

oscillation, but this is not correct. For the walking test shown in Figure 2.25, the floor bay has two very responsive modes, one at 6.4 Hz and one at 8.1 Hz. A walking test was performed at 2.13 Hz (128 bpm) in an attempt to cause resonance using the third harmonic of walking (3x2.13 Hz = 6.4 Hz). However, the fourth harmonic frequency is fairly close to the 8.1 Hz modal frequency, so some of the energy was applied at 8.1 Hz, causing resonance with that mode also, as shown in Figure 2.25(c). The walking acceleration waveform shown in Figure 2.25(b) seems to indicate that the footstep literally strikes the slab every third *and* every fourth oscillation which is obviously impossible.

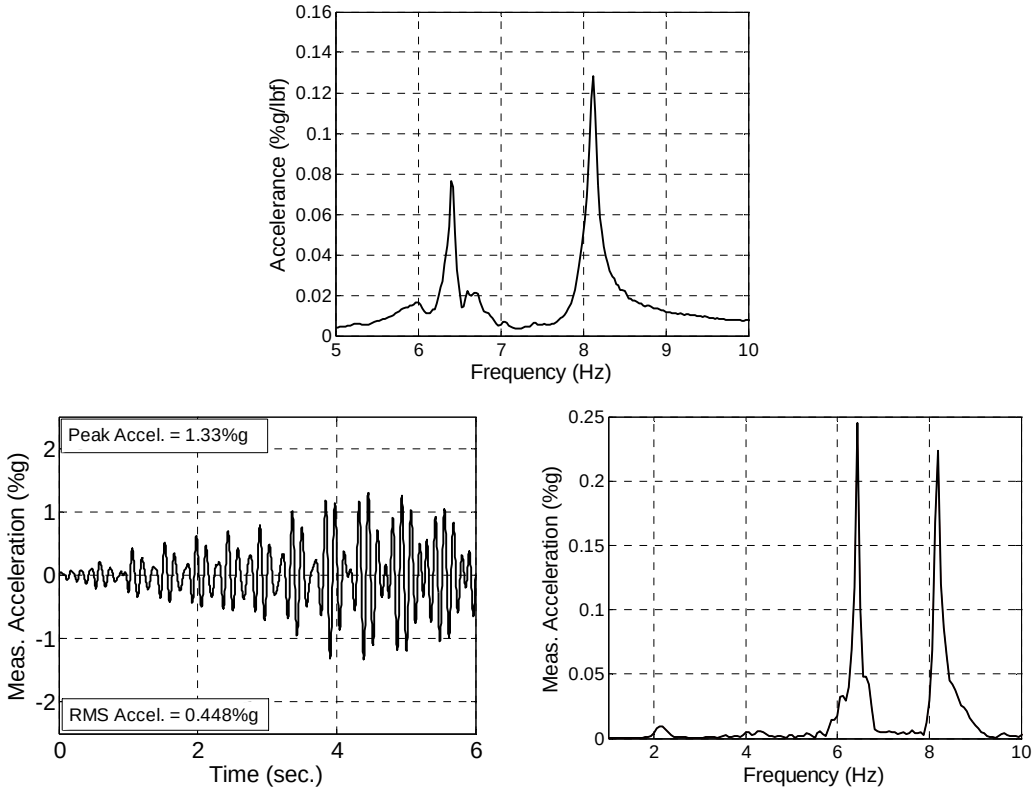

Figure 2.25: Sample Walking Test Illustrating Excitation of Two Significant Modes

The acceleration spectra shown in Figure 2.24 and Figure 2.25 also illustrate the imperfect nature of human walking. If the walker accomplished a step frequency exactly equaling the natural frequency subharmonic with identical footsteps, then the acceleration spectrum peak would be very narrow, approaching zero width. In reality, despite his best efforts, the walker's steps were at approximately equal intervals, but there was variability from step to step. Variability also undoubtedly existed in the individual footstep forces.

The result is that energy was spread over small bandwidths surrounding each walking harmonic frequency. This explains the surprising consistency that is seen in walking test results even for very lightly damped floors. Consider the narrowness of the FRF magnitude shown in the Figure 2.26, which is typical for the presented research. The critical modal damping ratio was 0.436%. The FRF magnitude at very small deviations from the natural frequency are significantly lower than at the peak. At 0.025 Hz below and 0.050 Hz above the natural frequency, the peak magnitudes are 38% and 52% lower than at the natural frequency. Therefore, one might anticipate that several walking tests would produce very different peak accelerations, but this was not observed during this research. Instead, when multiple tests were performed, several tests usually had similar high levels of response. The footstep force harmonic undoubtedly was spread over a narrow bandwidth at the natural frequency, allowing a similar response from test to test.

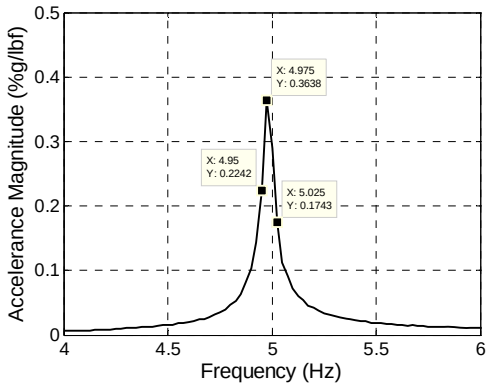

Figure 2.26: FRF Illustrating Narrowness of Peak

2.4 Footstep Force Definitions

The main objective of this research was to develop a method of predicting floor vibration response to walking using finite element modeling procedures. Toward that goal, footstep forces were measured and processed to define direct and rational loading functions. The general approach was to define an individual footstep force waveform that can be applied to nodes in the model at specific times and locations for use during response history analyses. This section describes the measurements, waveform selection process, and issues associated with the chosen approach.

2.4.1 Footstep Force Measurement

Individual footstep force measurements were recorded in the Virginia Tech Engineering Science and Mechanics Department's Biomechanics Laboratory using a Bertec 9090 force platform (Bertec Corp, Columbus OH) as shown in Figure 2.27. The goal was to measure single step forcing functions to obtain a representative footstep or set of footsteps for application in finite element models.

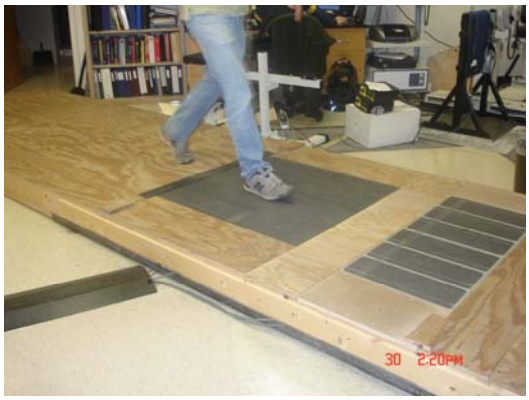

Figure 2.27: Footstep Force Measurement

Using the force platform, several footstep force measurements were recorded for each of the three walkers. Step frequencies were selected at a 5 bpm interval from 90 bpm to 130 bpm, to encompass the reasonable range of step frequencies. Several measurements were taken at each step frequency to assess repeatability and to provide footsteps with various frequency contents. All walkers had "normal" walking patterns, or gaits, unaffected by physical abnormalities, and wore the same shoes that were worn during walking acceleration tests discussed in a previous section. (However, as mentioned previously, the choice of shoes does not significantly affect the lower frequency content of footfall forces.) Footsteps were assumed to be equal for the left and right feet, so no effort was made to record which foot applied the measured footstep. While small differences may exist between the left and right feet, this approximation has been used by previous researchers (Kerr and Bishop 2001, Ellingwood and Tallin 1984). A sample recorded footstep is shown in Figure 2.28.

When analyzing the data, it was found that footsteps that look very similar in the time domain can result in very different predicted responses. Therefore, a rational selection criterion was developed. Floor bays are divided into two broad categories: low frequency floors and high frequency floors, with 10 Hz typically considered to be the

frequency that divides the two groups. Separate selection criteria must be used for these two groups because their fundamental behaviors are different. Low frequency floors are subject to resonant build-ups whereas high frequency floors are not. Footsteps for use with low frequency floors must be selected based on frequency content whereas footsteps for use with high frequency floors must be selected based on response to individual footsteps. All of the floors in this research were low frequency floors, so the footsteps defined herein are applicable only to such floors. It is unknown whether the same footsteps are also appropriate for high frequency floors.

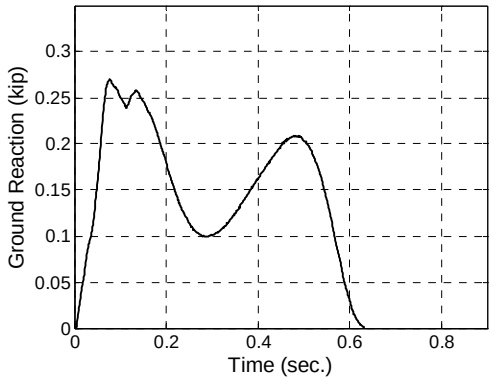

Figure 2.28: Sample Footstep Force Waveform, 120 bpm

Before selection of footsteps was possible, reasonable frequency content was established. The database presented by Willford et al. (2007), based primarily on the research by Kerr (1998), provides a statistical basis for selecting reasonable frequency content. They plotted the footstep force Dynamic Load Factors (DLF – Ratio of Fourier series sinusoidal amplitude to bodyweight) for the first four harmonics versus frequency and used linear regression to determine mean and 75th percentile force levels as functions of frequency. The 75th percentile force levels are considered a "design" level of force and form the basis of the SCI DG forcing functions for low frequency floors as shown in Figure 2.29. To remain consistent with the SCI DG, footsteps were selected based on the "design" level force.

Numerous footsteps were measured at each step frequency. The 120 bpm raw data is shown in Figure 2.30(a) and two of the individual footsteps are plotted in Figure 2.30(b) and Figure 2.30(c). These two footsteps look very similar in the time domain, but

produce very different responses when used as loading functions in response history analyses because the frequency content of these two footsteps are very different.

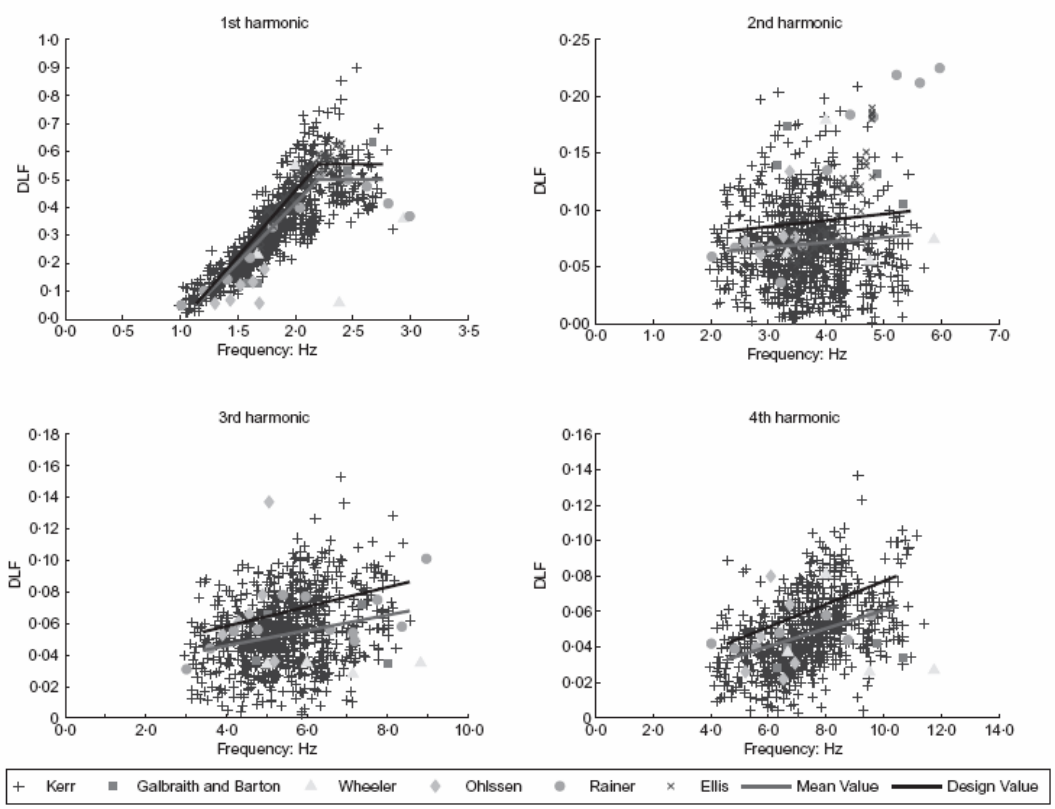

Figure 2.29: Footstep Force Harmonics (Willford et al. 2007)

The frequency content of each individual footstep was computed using a discrete Fourier transform. To accomplish this for a specific footstep, the footstep was placed in a series and superimposed as shown in Figure 2.31(a). A perfectly repeating portion of the waveform was then selected and used to compute the frequency content, satisfying the first DFT (Discrete Fourier Transform) assumption: periodicity. Figure 2.31(b) shows a repeating portion, which is arbitrary. Any repeating portion of the waveform could be selected and the same result obtained, which was verified during data processing. Note that if the repeating portion is not precisely selected, then the resulting DFT will have non-zero magnitudes at frequencies other than the step frequency and step frequency harmonics.

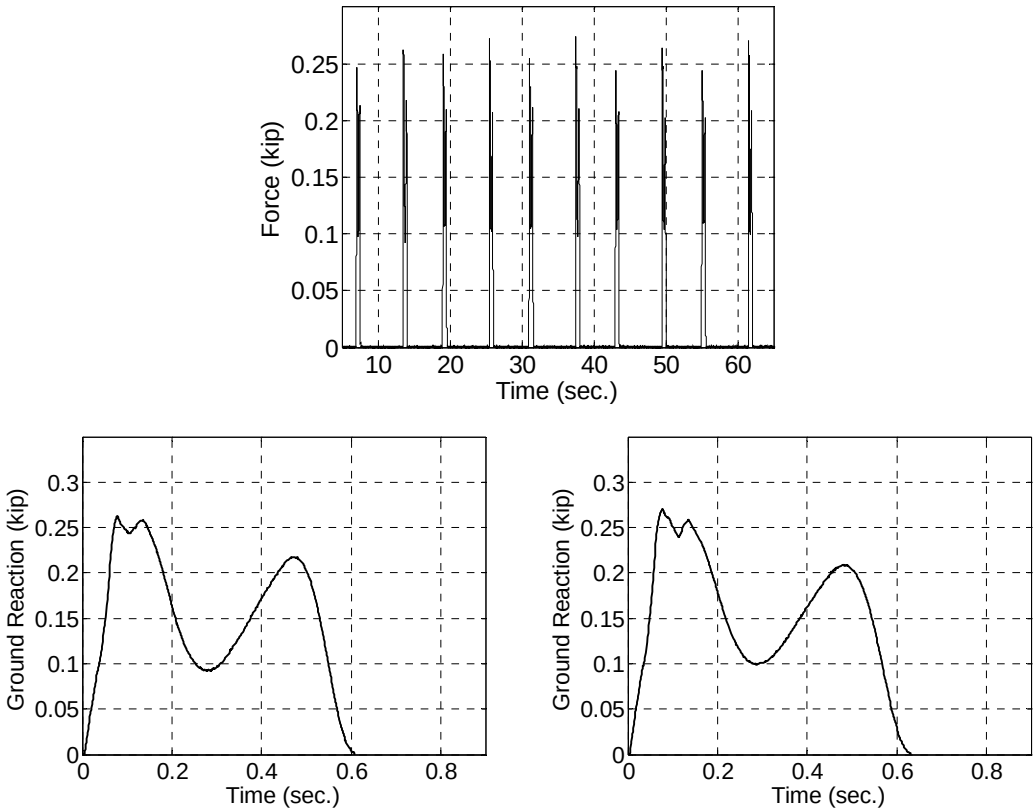

Figure 2.30: Sample Footstep Measurements (120 bpm). (a) Raw Data; (b) Sample Individual Step; (c) Sample Individual Step

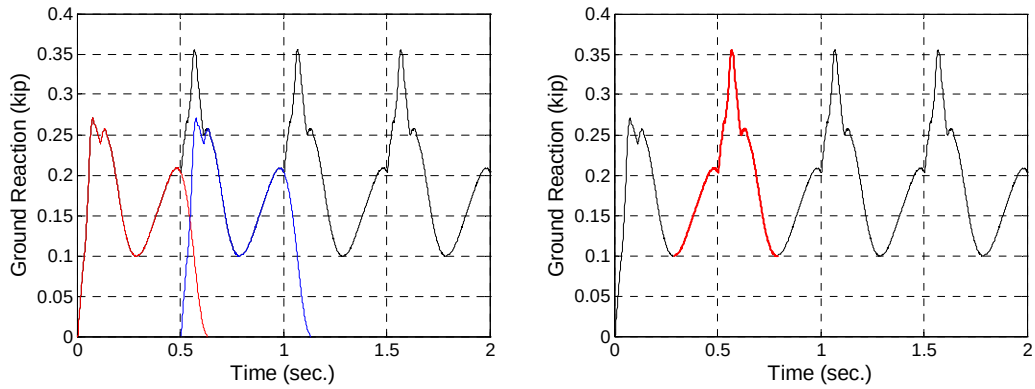

Figure 2.31: Footstep Series. (a) Superposition; (b) Repeating Portion

The DFT magnitude was computed for each footstep series and divided by the walker's bodyweight to determine a normalized frequency content, hereafter referred to as a DLF to be consistent with the literature. The magnitude was used as the selection criterion without respect to the DFT phase because the footsteps will be applied to force *one* harmonic to match a natural frequency. Excitation of multiple modes is possible in

reality (Figure 2.25), but it is currently not possible to reliably predict multiple modes at the correct order and at the correct frequency spacing. Therefore, including the phase as a selection criterion seems to add significant difficulty without benefit.

The DLFs for the two footsteps shown in Figure 2.30(b) and (c) are shown in Figure 2.32. The solid lines shown on the plots are the design DLFs defined by Willford et al. (2007), discussed earlier. The "Ratio" is the computed DLF divided by the design DLF. Even though the footstep waveforms look similar in the time domain, their third and fourth harmonic magnitudes are 3.5 and 2.1 times different, respectively. The footstep frequency contents proved to be extraordinarily sensitive to very small differences in shape, as illustrated here. The second footstep shown was the closest match of all the 120 bpm footsteps measured and has frequency content within approximately 20% of the design DLFs. It proved impossible to select footsteps that had all of the first four harmonic DLFs approximately equal to the design DLFs. The first harmonic was excluded from the comparisons because it is not possible to have any reasonable floor structure with a natural frequency within reach of the first harmonic (approximately 2.2 Hz). The second harmonic can excite a few floors, but the third and fourth harmonics excite the vast majority. Therefore, they were used as the primary selection criteria. The second harmonic is on the conservative side for every footstep.

It was necessary to define footsteps at each 5 bpm increment from 90 bpm to 135 bpm because the DLFs drift when the footstep is applied at other step frequencies. For example, the 120 bpm footstep has slightly different DLFs when applied at 118 bpm. The DLFs drift by unacceptably large amounts when the footstep frequency is varied by more than approximately 2.5 bpm from the measured step frequency. In other words, the 120 bpm footstep has acceptable frequency content only between approximately 117.5 bpm and 122.5 bpm.

At three frequencies (105 bpm, 115 bpm, and 130 bpm), it was not possible to select a footstep from the measurements that had DLFs acceptably close to the design DLFs. In these cases, the footsteps were "improved" by determining the frequency content, forcing the DLFs to match the design DLFs and re-synthesizing an improved footstep series using an inverse DLF (IDLF). This was only partially successful, however, because it is not possible to directly determine an improved initial part (first

approximately 0.1 sec. shown in Figure 2.33) and last part of the footstep force waveform. The original footstep initial and last parts were used, which caused the improved DLFs to vary somewhat from the design DLFs. They are improved to within acceptable deviation from the design DLFs. The process is illustrated in Figure 2.33 for the 105 bpm footstep. Figure 2.33 shows the minuscule difference in waveform required to cause very significant differences in DLFs.

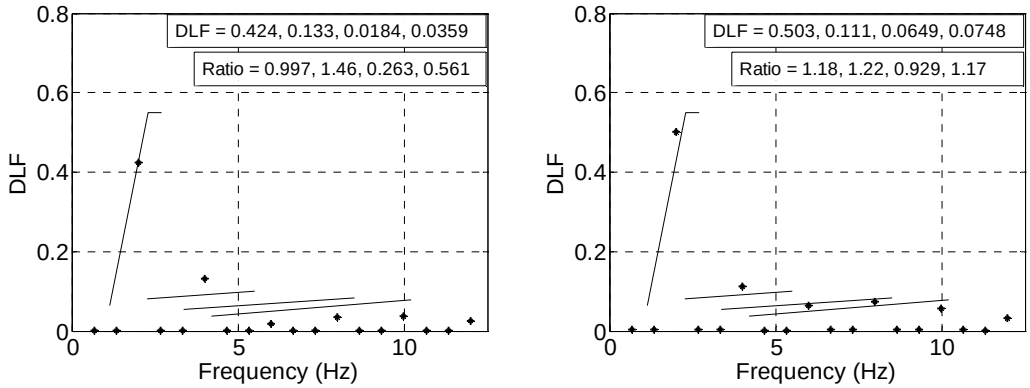

Figure 2.32: DLFs for Two 120 bpm Measured Footsteps

The final selected design footstep waveforms and corresponding DLFs are shown in Figure 2.34. These footsteps, scaled to have average DLFs rather than 75th percentile design DLFs, were used in the in the finite element models to predict floor vibration response in Chapter 4.

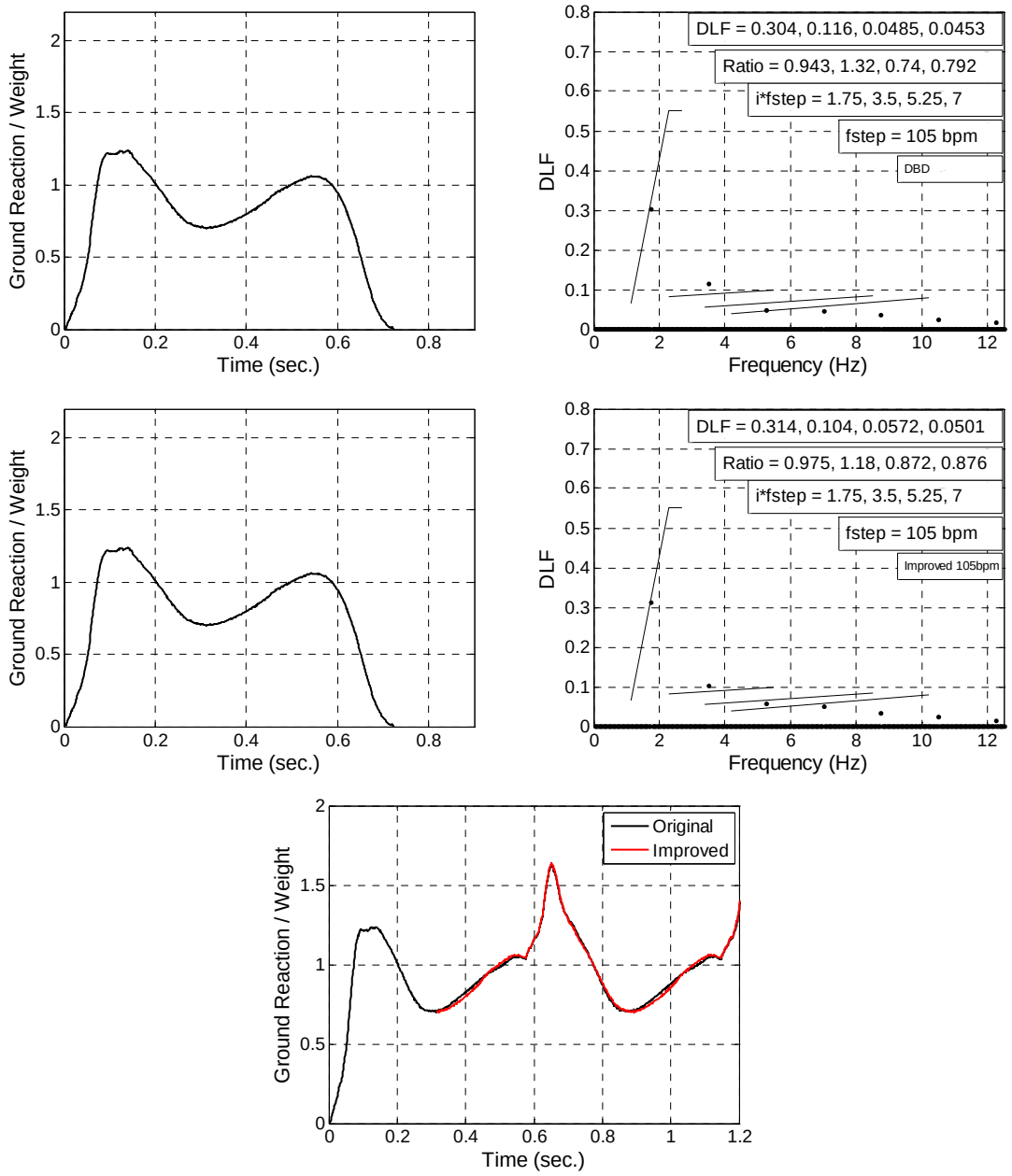

Figure 2.33: 105 bpm Design Footstep. (a) Original Waveform; (b) Original DLF; (c) Improved Waveform; (d) Improved DLF; (e) Original and Improved Waveforms

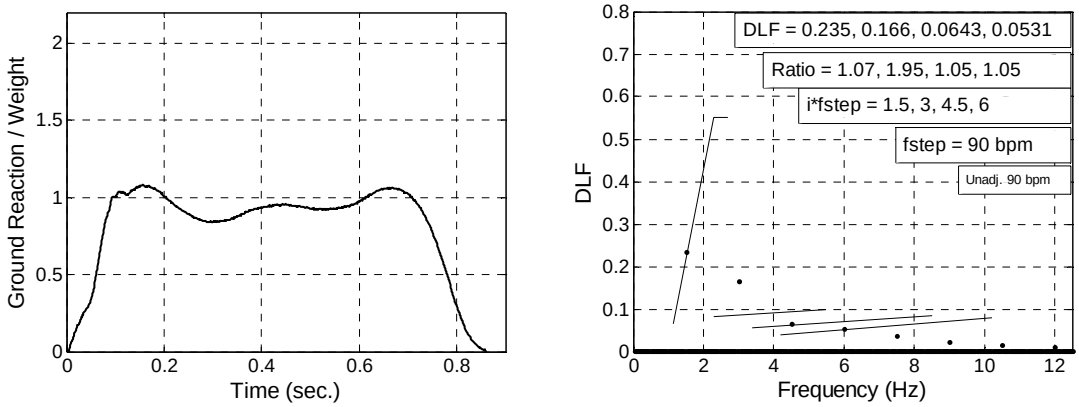

(a) 90 bpm Design Footstep

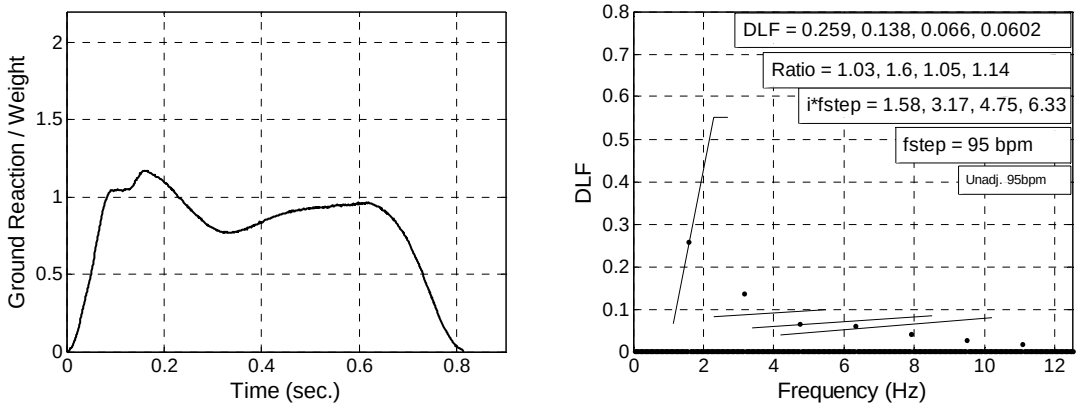

(b) 95 bpm Design Footstep

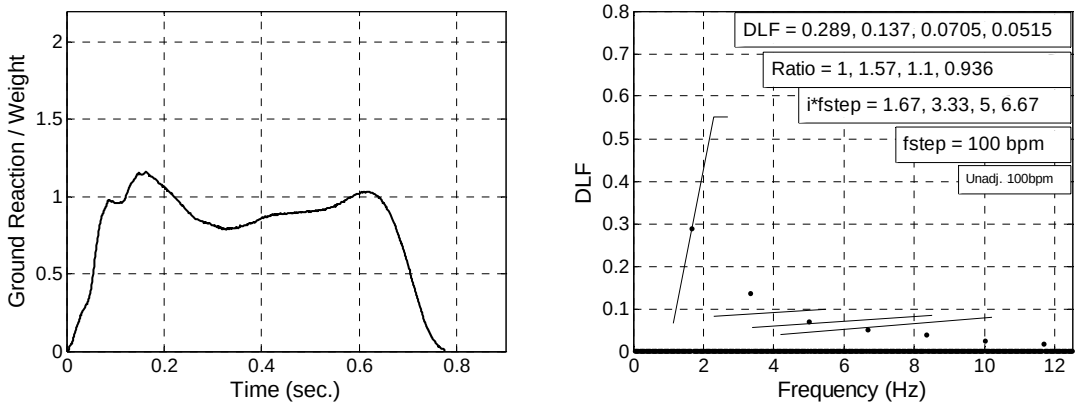

(c) 100 bpm Design Footstep

Figure 2.34: Design Footstep Waveforms and DLFs

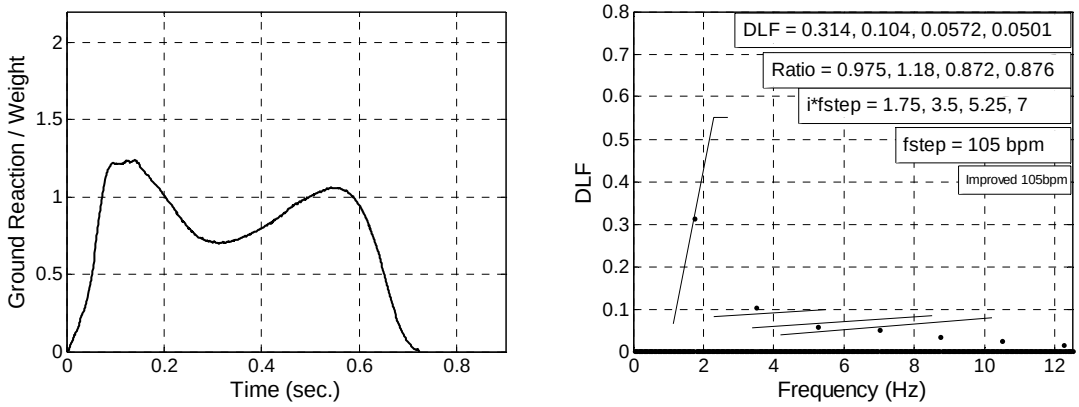

(d) 105 bpm Design Footstep

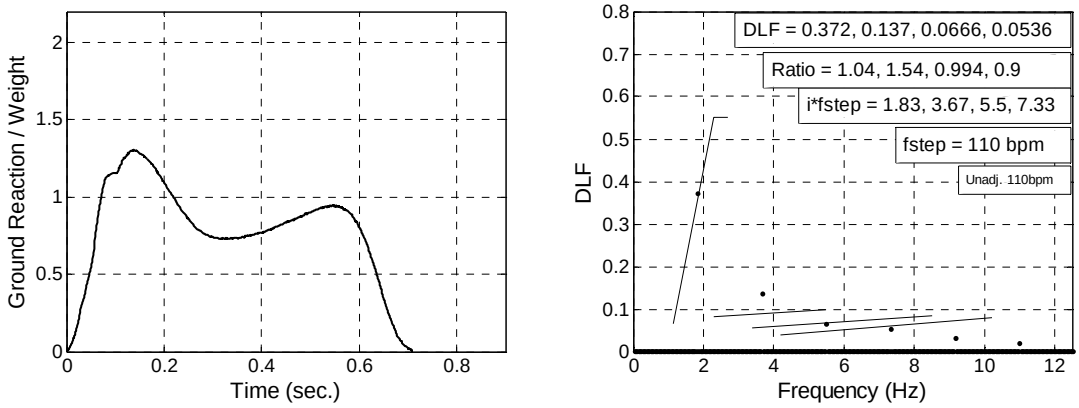

(e) 110 bpm Design Footstep

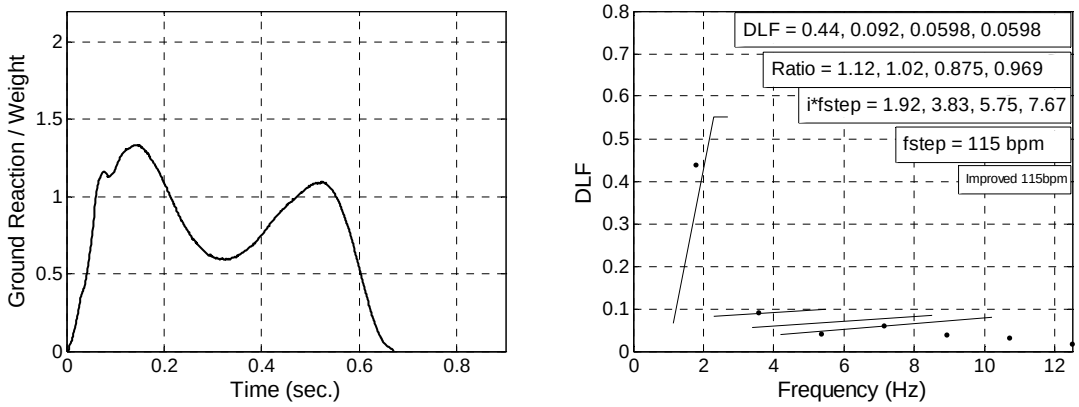

(f) 115 bpm Design Footstep

Figure 2.34: Design Footstep Waveforms and DLFs (continued)

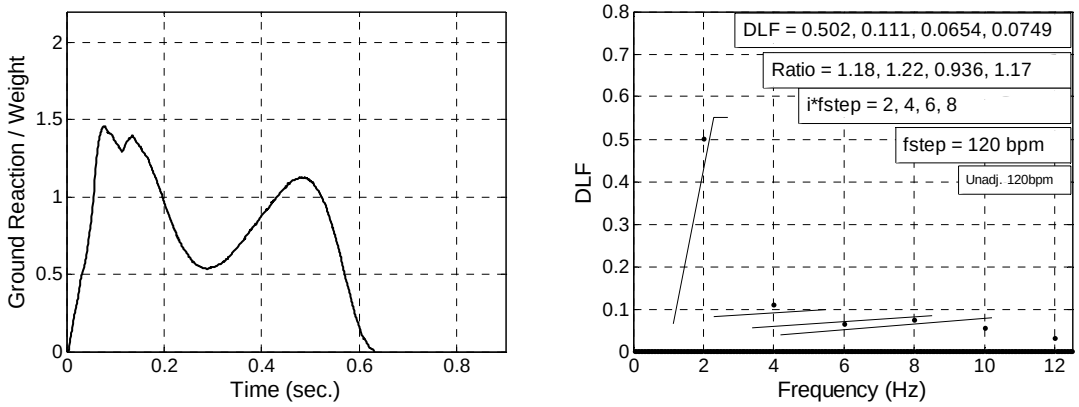

(g) 120 bpm Design Footstep

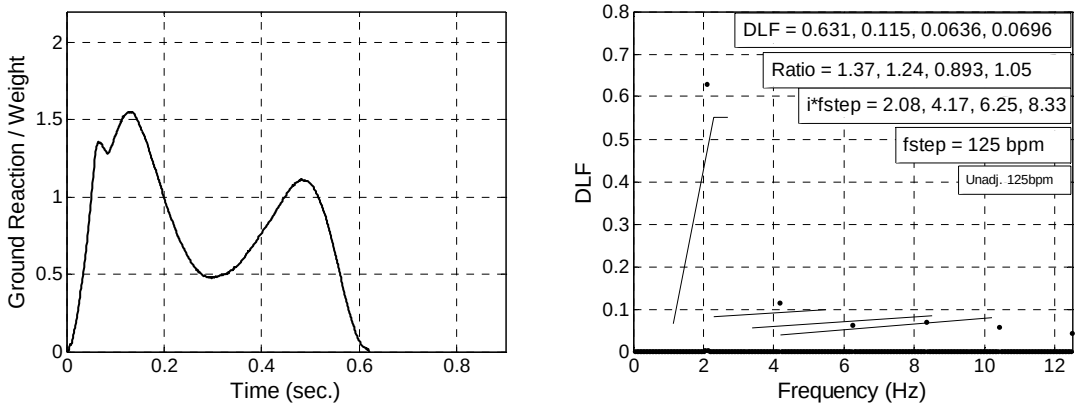

(h) 125 bpm Design Footstep

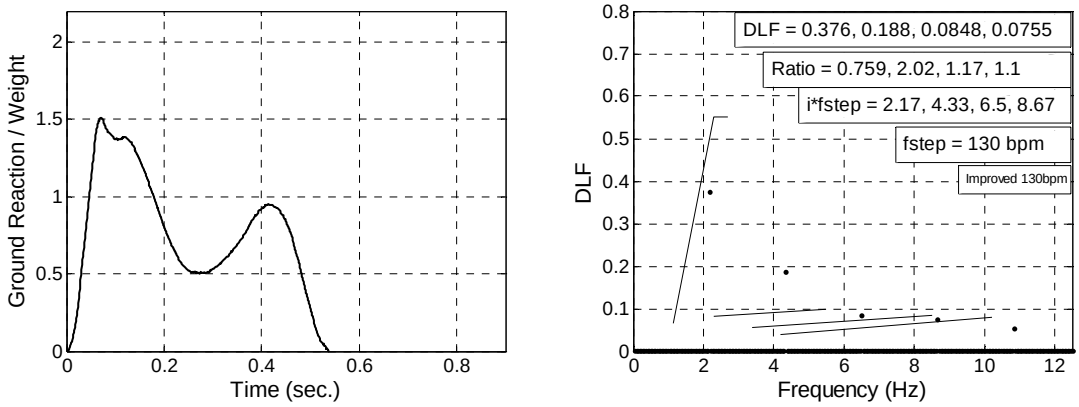

(i) 130 bpm Design Footstep

Figure 2.34: Design Footstep Waveforms and DLFs (continued)

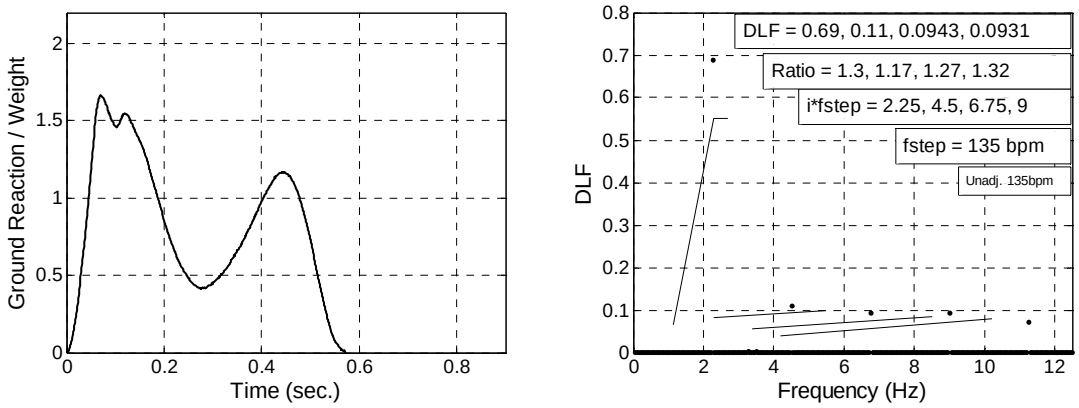

(j) 135 bpm Design Footstep

Figure 2.34: Design Footstep Waveforms and DLFs (continued)